文章编号： 1007-8827(2017)05-0442-09

# 不粘煤基活性炭作超级电容器电极材料：硼、氮掺杂对其电化学性能的影响

陆 倩[1]， 徐园园[1]， 木沙江[2]， 李文翠[1]
(1. 大连理工大学 化工学院，精细化工国家重点实验室，辽宁 大连 116024；
2. 新疆煤炭科学研究所，新疆 乌鲁木齐 830091)

**摘 要：** 以新疆不粘煤为原料，三聚氰胺为氮源，硼酸为硼源，通过球磨和后续活化过程合成硼，氮掺杂及硼氮共掺杂煤基活性炭。氮吸附结果显示杂原子掺杂可提高活性炭中介孔的含量。红外和 X 光电子能谱结果显示，硼、氮原子存在于炭骨架中。循环伏安，恒流充放电及电化学阻抗分析说明硼、氮掺杂活性炭的电化学性能优于非掺杂活性炭。其中，硼氮共掺杂活性炭具有 176 $F\cdot g^{-1}$ 的高比容量。循环 20 000 次容量保持率为 96%。共掺杂活性炭优异的电化学性能归因于硼氮的协同作用。

**关键词：** 活性炭；杂原子掺杂；超级电容器；电化学性能
**中图分类号：** TQ127.1+1 **文献标识码：** A

基金项目：国家自然科学基金（NSNF，U1303192）；新疆维吾尔族自治区自然科学基金项目（2012211A108）.
通讯作者：李文翠，教授. E-mail：wencuili@dlut.edu.cn
作者介绍：陆 倩，硕士研究生.

# The effect of nitrogen and/or boron doping on the electrochemical performance of non-caking coal-derived activated carbons for use as supercapacitor electrodes

LU Qian[1]， XU Yuan-yuan[1]， MU Sha-jiang[2]， LI Wen-cui[1]
(1. *State Key Laboratory of Fine Chemicals*, *School of Chemical Engineering*, *Dalian University of Technology*, *Dalian* 116024, *China*;
2. *Xinjiang Coal Research Institute*, *Urumqi* 830091, *China*)

**Abstract:** Coal-based activated carbons doped with either N or B or a combination of the two were prepared for use as the electrode materials of supercapacitors by ball milling and subsequent activation using Xinjiang non-caking coal, melamine and boric acid as the respective carbon, nitrogen and boron sources. FTIR spectroscopy and XPS reveal that the B and N atoms are substitutionally incorporated into the carbon skeleton. These doped activated carbons contain a large number of mesopores. Cyclic voltammetry, galvanostatic charge/discharge and electrochemical impedance spectroscopy show that N- and B-doped activated carbons have a superior capacitance and rate performance to the non-doped one. The B-N co-doped material has the highest specific capacitance of 176 $F\cdot g^{-1}$ at 0.5 $A\cdot g^{-1}$, which is attributed to a synergistic effect of B-N co-doping. The capacitance of the co-doped sample remains at 96% of the original value after 20 000 cycles.

**Key words:** Activated carbon; Heteroatom-doping; Supercapacitor; Electrochemical performance

*Received date*: 2017-04-25; *Revised date*: 2017-08-01
*Foundation item*: National Natural Science Foundation of China (NSNF, U1303192); Natural Science Fund Project of Xinjiang uighur autonomous region (2012211A108).
*Corresponding author*: LI Wen-Cui, Professor. E-mail: wencuili@dlut.edu.cn
*Author introduction*: LU Qian, Master Student.
English edition available online ScienceDirect ( http://www.sciencedirect.com/science/journal/18725805 ).
DOI: 10.1016/S1872-5805(17)60133-1

## 1 Introduction

One of the modern trends in the use of energy sources is the creation of highly efficient portable energy storage devices, such as batteries, supercapacitors and fuel cells[1]. Among current energy storage devices, supercapacitors have attracted much attention owing to their long cycle life, high power density, great stability and good reversibility[2,3]. Porous car-

bon materials, usually prepared from physical and/or chemical activation of carbonaceous precursors, have a high surface area, well-developed porosity and good electrical conductivity, and have been extensively considered as electrode materials for supercapacitors[4].

Physical activation usually refers to the treatment of carbon precursors at high temperature (600 ~ 1 200 ℃) in the presence of oxidizing gases such as steam, $CO_2$ and air. Chemical activation is carried out when carbonaceous precursors are mixed with chemical agents like KOH, $H_3PO_4$ and $ZnCl_2$, and treated at 400- 900 ℃[5-7]. The chemical activation generates abundant micropores at a high efficiency, while the physical activation is more beneficial to create small mesopores. It is well known that the existence of a certain amount of mesopores in activated carbons (ACs) is advantageous to achieve a high rate performance for supercapacitors. Not only surface area and pore size distribution are important parameters for the performance of supercapacitor, but also some other aspects of the carbon materials such as surface chemistry and electrical conductivity that also influence their electrochemical performance to a great extent.

It has been proved that carbons doped with electron-donating or electron-withdrawing heteroatom on skeleton, such as nitrogen[8-12], boron[13-17], phosphorus[18], sulfur[19], boron-nitrogen (B—N)[20-23], nitrogen-sulfur (N—S)[24] and nitrogen-phosphorus (N—P)[25, 26] present outstanding electronic properties. Additionally functional groups on the carbon surface can enhance the wettability of electrodes, markedly resulting in a high surface utilization and pore accessibility.

In this report, B, N-doped and B—N co-doped ACs prepared by a solid-state ball milling and subsequent activation were evaluated for their capacitive behavior. Xinjiang non-caking coal was used as a carbon precursor. This type of coal is especially suitable for electrode materials because of its non-viscous property and low ash content. Boric acid and melamine were used as boron and nitrogen source, respectively. The obtained heteroatom doped ACs were used as an electrode material for supercapacitors and the effect of the heteroatom doping on electrochemical performance was studied. The results show that B-N co-doped ACs exhibit the highest capacitance of 176 $F \cdot g^{-1}$ at 0.5 $A \cdot g^{-1}$, owing to their well-developed porosity and surface chemistry. The co-doping of B and N for ACs and the resulting surface functional groups lead to the improved wettability between electrode and electrolyte. After 20,000 cycles, its capacitance retention rate remains 96% of the original value.

## 2 Experimental

### 2.1 Materials and chemicals

The Xinjiang coal was provided by the Xinjiang Coal Science Research Institute. Melamine (AR, 99.0%) was purchased from Sinopharm Chemical Reagent Co., Ltd. Boric acid (AR) was purchased from Tianjin Kermei Chemical Reagent Co., Ltd. Potassium hydroxide (GR, 95%) was supplied by Aladdin Industrial Corporation.

### 2.2 Preparation of N-doped, B-doped and B, N-co-doped ACs

The Xinjiang coal was crushed and sieved to a size of 80-100 mesh, carbonized at 650 ℃ for 2 h, and washed with hydrochloric acid and sodium hydroxide. The ash content of the resulting sample was 0.39 wt% by the proximate analysis method of coal (GB/T 212-2008). The obtained sample was denoted CC. The proximate and ultimate analysis of the Xinjiang coal are shown in Table 1.

**Table 1　Proximate and ultimate analysis of the Xinjiang coal (wt. %).**

| Proximate analysis | | | | Ultimate analysis | | | | |
|---|---|---|---|---|---|---|---|---|
| $M_{ad}$ | $A_{ar}$ | $V_{daf}$ | $F_{Car}$ | $C_{ar}$ | $H_{ar}$ | $O^*_{ar}$ | $N_{ar}$ | $S_{t,ar}$ |
| 2.28 | 3.97 | 35.47 | 58.48 | 78.89 | 4.48 | 15.68 | 0.60 | 0.35 |

$M_{ad}$: moisture, $A_{ar}$: ash, $V_{daf}$: volatiles, $F_{car}$: fixed carbon, $O_{ar}{}^*$: the oxygen is assessed by difference.

For the preparation of N-doped AC, 2 g of melamine and 2 g of CC were mixed thoroughly by ball-milling at 360 rpm for 90 min. Afterwards, the mixture was transferred into a crucible and placed in a tube furnace for activation under steam at 800 ℃ and 850 ℃ for 2 h using nitrogen as the carrier gas to obtain samples named as NAC-800 and NAC-850 respectively.

The synthesis of B-doped and B, N co-doped ACs was similar to the N-doped one. In the case of B-doped AC, 2 g of boric acid and 2 g of CC were ball-milled. While, in the case of B, N co-doped AC, 1 g of boric acid, 1 g of melamine, and 2 g of CC were ball-milled. After activation, the samples were treated with 2 L of hot water to wash away any boron oxide. After drying, heteroatom-doped ACs

were obtained and denoted as BAC-800, BAC-850 and BNAC-850 accordingly. As a contrast, AC was prepared from the carbonized Xinjiang coal CC, without any heteroatom doped, and denoted as AC.

### 2.3 Characterization

Nitrogen sorption isotherms were measured with a Micromeritics tristar 3000 instrument adsorption analyzer at 77.4 K. Before measurement, samples were degassed under vacuum at 200 ℃ for 4 h. The Brunauer-Emmett-Teller (BET) method was used to calculate the specific surface areas ($S_{BET}$). Total pore volumes ($V_{total}$) were calculated from the cumulative amount of nitrogen adsorbed at a relative pressure ($P/P_0$) of 0.99. Micropore volumes ($V_{micro}$) were calculated using the t-plot method. X-ray photoelectron spectroscopy (XPS) was performed using an ESCALAB250. Elemental analysis was implemented on a CHNO elemental analyzer (Vario EL Ⅲ, Elementar). The boron content was obtained from inductively coupled plasma optical emission spectrometry (ICP). The functional groups of the samples were characterized by Fourier transform infrared spectroscopy (FTIR).

### 2.4 Electrochemical measurements

The working electrode was made by mixing 80 wt% of ACs, 10 wt% of conductive carbon black and 10 wt% of polytetrafluoroethlene (PTFE). Subsequently, the mixture was dispersed in a solvent mixture containing 2 mL ethanol and 1 mL $H_2O$. The slurry was rolled into a film, followed by dehydration at 120 ℃ for 4 h. The film was placed on a nickel foam under 10 MPa for 5 min. The electrochemical test was carried out using a three electrode system with Hg/HgO as the reference electrode, as-prepared electrode as the working electrode and platinum plate as the counter electrode in a 6 M KOH electrolyte. The specific capacitance was calculated by the following equation:

$$C_m(F\cdot g^{-1}) = I\times\Delta t/(m\times\Delta V)$$

Where I, $\Delta t$, m and $\Delta V$ are the discharge current, the discharge time, the mass of active materials and the potential window (−1 V in this work), respectively. The energy density and power density were calculated from the following equations:

$$E(Wh\cdot kg^{-1}) = 1/2\ CV^2 \qquad P(W\cdot kg^{-1}) = E/t$$

where $C$ is the specific capacitance based on a two-electrode system, $V$ is the potential window from the end of the voltage drop to the end of the discharge process and t is the discharge time, respectively.

## 3 Results and discussion

### 3.1 Physical and chemical properties of the coal-based activated carbons

Nitrogen adsorption was applied to measure the porosity of the obtained samples. As shown in Fig. 1a, nitrogen adsorption isotherms of NAC-850, BAC-850 and BNAC-850 show a typical type IV isotherm with a hysteretic loop, indicating the characteristic of a mesoporous structure. NAC-800, BAC-800 and non-doped AC exhibit a type I isotherm, confirming their microporous structure[27].

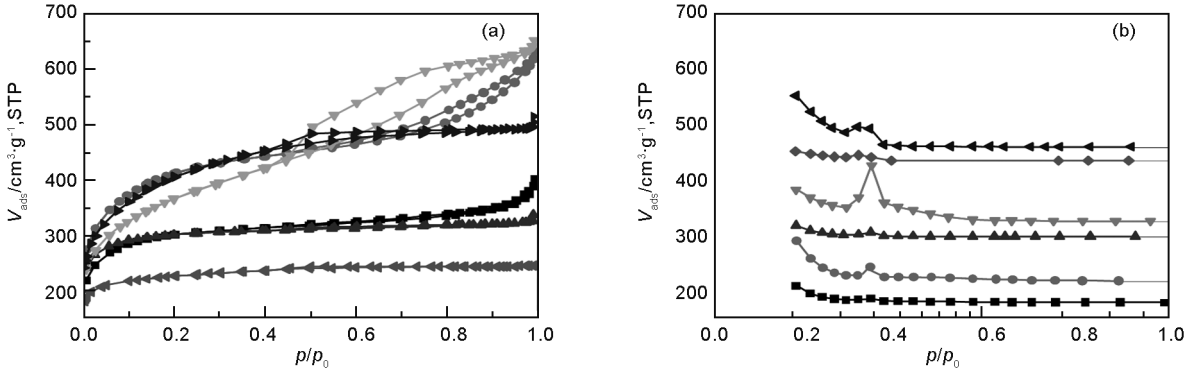


Fig. 1 (a) $N_2$ adsorption isotherms and (b) pore size distributions of the coal-based ACs.
■: AC; ●: NAC-850; ▲: NAC-800; ▼: BAC-850; ◆: BAC-800; ◄: BNAC-850

As shown in Table 2, NAC-850 exhibits the highest $S_{BET}$ of 1 436 $m^2\cdot g^{-1}$ and a $V_{meso}/V_{total}$ ratio of 71%, and NAC-800 shows an $S_{BET}$ of 1 022 $m^2\cdot g^{-1}$ and a $V_{meso}/V_{total}$ ratio of 28%. With an increase of activation temperature, a number of the as-formed micropores are further etched by steam to form mesopores. The N-doped sample has a higher $S_{BET}$ than the B-doped sample at the same activation temperature. Pore size distribution (PSD) curves (Fig. 1b) show that the mesopores of NAC-850, BAC-850 and BNAC-850 are centered at 3-5 nm. Samples with both micropores and mesopores are expected to have a good electrochemical performance as electrode materials, because micropores can provide a large surface area for adsorbing ions and mesopores provide channels for ions diffusion into the bulk of the material to

**Table 2　Textural parameters of Xinjiang coal-based activated carbons**

| Sample | $S_{BET}/m^2 \cdot g^{-1}$ | $S_{mic}/m^2 \cdot g^{-1}$ | $V_{total}/cm^3 \cdot g^{-1}$ | $V_{mic}/cm^3 \cdot g^{-1}$ | $V_{meso}/V_{total}/\%$ |
|---|---|---|---|---|---|
| AC | 1032 | 703 | 0.62 | 0.32 | 48 |
| NAC-850 | 1436 | 618 | 0.98 | 0.28 | 71 |
| NAC-800 | 1022 | 794 | 0.52 | 0.37 | 29 |
| BAC-850 | 1288 | 402 | 1.00 | 0.18 | 82 |
| BAC-800 | 792 | 616 | 0.38 | 0.27 | 29 |
| BNAC-850 | 1312 | 448 | 0.80 | 0.24 | 66 |

$S_{mic}$: micropore surface area; $V_{mic}$: micropore volume; $V_{meso}$: mesopore volume determined by subtracting $V_{mic}$ from $V_{tot}$.

access micropores.

The chemical composition and bonding of the heteroatom doped ACs were further characterized by FTIR as shown in Fig. 2. It is seen in Fig. 2 that the band at 3 440 $cm^{-1}$ is assigned to N—H or O—H stretching vibration. The bands at 1 640 and 940 $cm^{-1}$ are attributed to N—H in-plane stretching and out-plane stretching, respectively. The band at 1 380 $cm^{-1}$ is ascribed to B—N in-plane stretching. The band at 1 009 $cm^{-1}$ corresponds to B—C stretching[23, 27, 28]. Above mentioned results confirm the existence of N and B containing functional groups in the carbon framework.

XPS, ICP and elemental analysis were carried out to verify the surface and bulk element composition of the heteroatom-doped coal-based ACs. Table 3 shows the content of boron and nitrogen of the obtained carbons. For the N-doped ACs, the nitrogen content decreases with the activation temperature, indicating that nitrogen is thermodynamically more stable at a lower temperature than at a higher temperature[11]. In the case of the B-doped ACs, the influence of treatment temperature is contrast to the N-doped ACs. The higher the treatment temperature, the higher boron diffused into the carbon skeleton. In the case of the B-N co-doped AC (BNAC-850), the content of B and N both on the surface and in the bulk are more than those of single element doped ACs, which indicates that B and N can be stabilized by co-doping. XPS spectra and FTIR of the BNAC-850 below support this point.

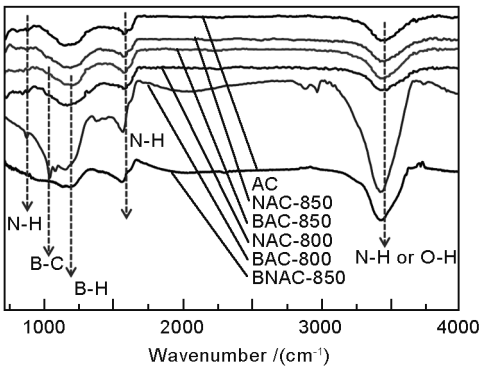


Fig. 2　FTIR spectra of AC, NAC-850, NAC-800, BAC-850, BAC-800, and BNAC-850.

**Table 3　Elemental analysis of the heteroatom-doped ACs.**

| Samples | Elemental analysis / wt % | | | | ICP / wt % | XPS / at % | | |
|---|---|---|---|---|---|---|---|---|
| | C | O* | N | H | B | N | B | O |
| NAC-850 | 84.22 | 14.34 | 0.85 | 0.59 | - | 0.7 | - | 5.03 |
| NAC-800 | 90.08 | 7.08 | 2.04 | 0.8 | - | 1.23 | - | 5.95 |
| BAC-850 | - | - | - | - | 0.68 | - | 0.95 | 10.98 |
| BAC-800 | - | - | - | - | 0.50 | - | 0.34 | 7.82 |
| BNAC-850 | 85.59 | 11.68 | 1.66 | 1.07 | 1.78 | 1.57 | 1.13 | 8.16 |

* The oxygen is assessed by difference.

Fig. 3a shows the N 1s spectrum of NAC-850, which can be split into three peaks: pyridine nitrogen (398.87 eV), quaternary nitrogen (400.86 eV) and pyridine nitrogen (403 eV). NAC-800 on the other hand has an additional peak, which is attributed to pyrrole-like nitrogen (400.02 eV). This is ascribed to the different stabilities of the nitrogen-containing structure at different activation temperatures[11, 29]. As to the B-doped samples of BAC-850 and BAC-800 (Fig. 3b), B1s has a peak concentrated at 191 eV, which is higher than that of pure boron (188 eV), indicating that the boron bonded to carbon in $sp^2$ carbon network[30]. The peak intensity of the BAC-850 is stronger than that of BAC-800 due to a higher boron content of BAC-850 obtained at a high activation temperature. In Fig. 3c, d, B and N are incorporated on the surface of carbon. The B1s spectrum of the BNAC-850 shows three pronounced peaks at 189 eV for B—C, 191.14 eV for B—N and 193.6 eV for B—O bonds[28,31]. Strong absorption peaks of 191.14 eV band suggests that B and N are mainly bonding as B—N, which implies the existence of B and N domains in the B-N co-doped AC.

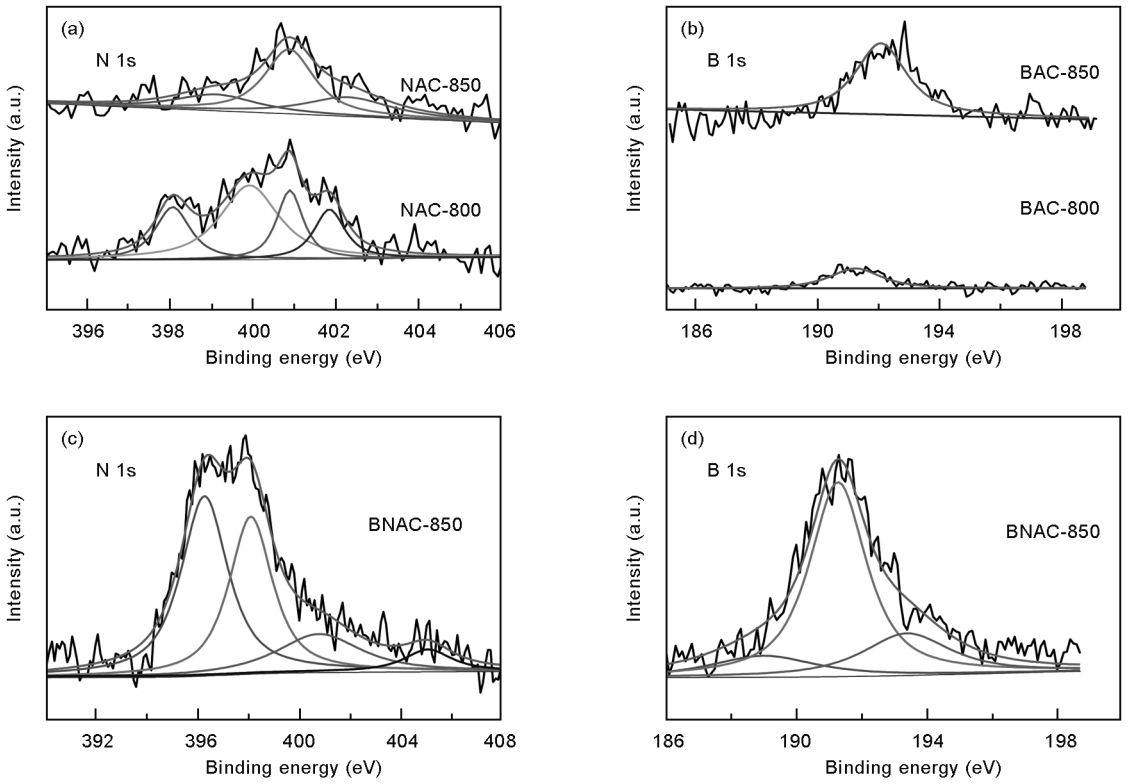


Fig. 3 XPS spectra of (a) N 1s of NAC-850 and NAC-800, (b) B 1s of BAC-850 and BAC-800, (c) N 1s and B 1s (d) of BNAC-850.

### 3.2 Electrochemical performance

Electrochemical tests, such as cyclic voltammetry (CV), galvanostatic charge/discharge (GC) and electrochemical impedance spectroscopy (EIS) are carried out in a three-electrode system in a 6 $mol \cdot L^{-1}$ KOH electrolyte and at a potential window from −1 to 0 V. Fig. 4a shows the CV curves of AC, NAC-850 and NAC-800 at a scan rate of 5 $mV \cdot s^{-1}$. CV curves of all samples present the characteristics of electrochemical double layer capacitor (EDL). NAC-850 exhibits an ideal rectangular-like shape of CV curves with an obvious hump (at ~0.4 V) which is attributed to a redox reaction of nitrogen containing functional groups. As shown in Fig. 4b, the specific capacitances of AC, NAC-850 and NAC-800 are 108, 156, 140 $F \cdot g^{-1}$ at 0.5 $A \cdot g^{-1}$, respectively. NAC-850 shows the largest specific capacitance due to the introduction of nitrogen containing functional groups and the highest specific surface area. And meanwhile the N-doping improves the wettability between electrode and electrolyte[32]. The specific capacitance of NAC-850 reaches a high value of 113 $F \cdot g^{-1}$, even at a high current density of 10 $A \cdot g^{-1}$.

Electrochemical impedance spectroscopy (EIS) data was analyzed by Nyquist plots as shown in Fig. 4c, which reflect the frequency response of the electrode/electrolyte system. The plots can be divided into two parts: a semicircle in the high frequency range and a steep line closing to 90° in the low frequency range. The intersection on the X axis corresponds to the equivalent series resistance (ESR), which consists of the resistance between current collector and active materials and the resistance of electrode. The radius of the semicircle represents the charge transfer resistance ($R_{ct}$) and the slope line in the low frequency range represents ideal capacitive properties[33, 34]. It can be seen that NAC-850 has the lowest ESR and steepest curve in the low frequency range, indicating the highest electrical conductivity compared to the other two samples. Cycling stability of NAC-850 was evaluated at a current density of 1 $A \cdot g^{-1}$ by assembling two symmetrical electrodes into one test cell. The specific capacitance of sample NAC-850 exhibits no decay after 20 000 cycles, as shown in Fig. 4d.

In Fig. 5a, it can be seen that B-doped ACs exhibit larger capacitances than AC, with two humps at around −0.4 and −0.8 V, which are the characteristics of the reversible redox reactions. The specific capacitance is contributed from EDL capacitance and pseudocapacitance stemming from the boron doping. As shown in Fig. 5b, BAC-850 has a capacitance of 132 $F \cdot g^{-1}$ compared to 119 $F \cdot g^{-1}$ for BAC-800 at a

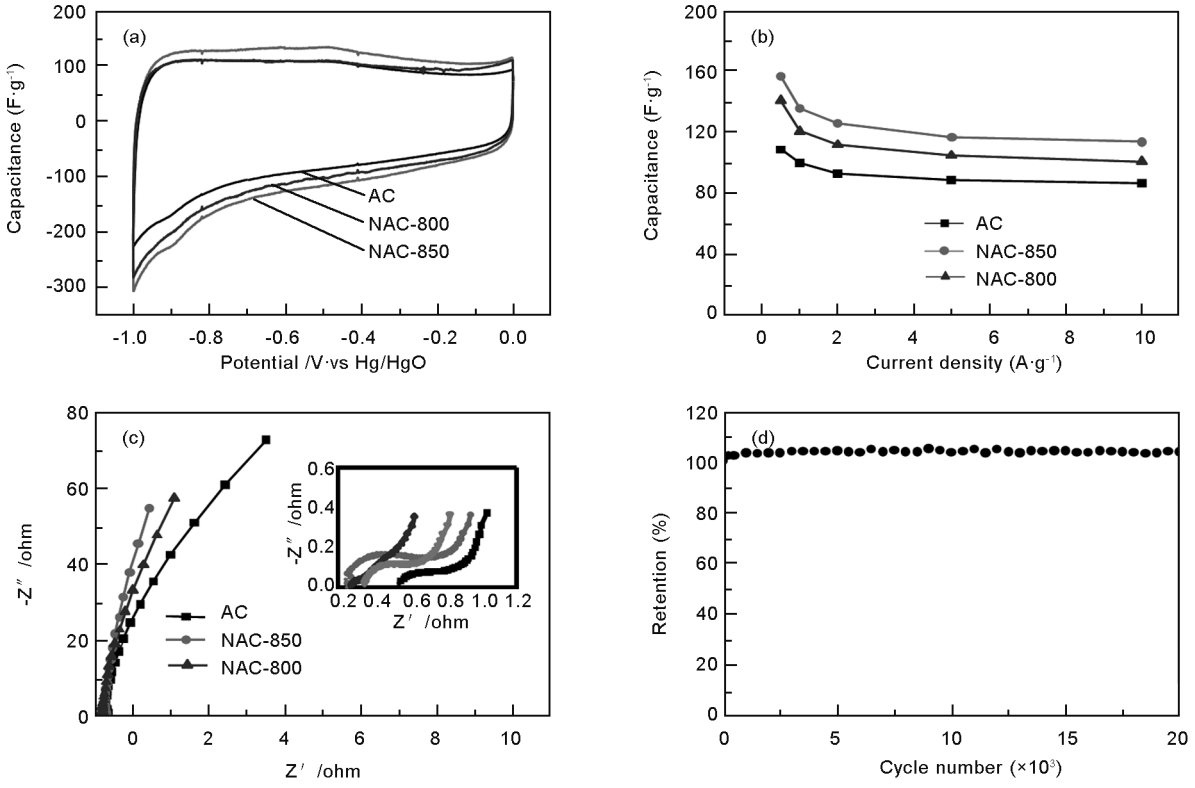


Fig. 4　The electrochemical performances of samples AC, NAC-800 and NAC-850, (a) CV curves recorded at a scan rate of 5 $mV \cdot s^{-1}$, (b) the specific capacitance as a function of discharging current density, (c) EIS and (d) cycling stability of NAC-850 at 1 $A \cdot g^{-1}$.

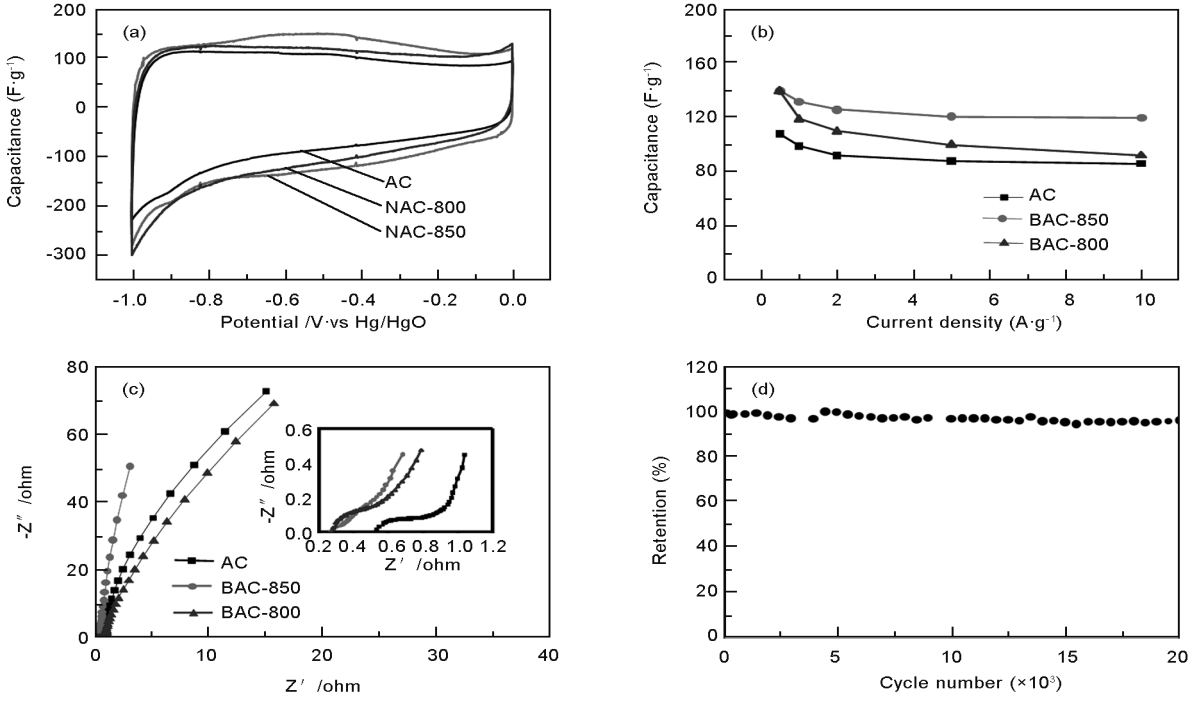


Fig. 5　The electrochemical performances of samples AC, BAC-800 and BAC-850, (a) CV curves recorded at 5 $mV \cdot s^{-1}$, (b) the specific capacitance as a function of discharging current density, (c) EIS and (d) cycling stability of BAC-850 at 1 $A \cdot g^{-1}$.

current density of 1 $A \cdot g^{-1}$ due to the high specific area and boron content of the former. Boron doping leads to changes of electronic properties and creates more electrochemically active sites on ACs. The charge density and the density of states at the Fermi level can be enhanced by replacing carbon atom with

boron atom because carbon atom has one more valence electron than boron atom[35-37]. In this case, charge transfer rate as well as the capacitive performance can be improved. On the other hand, oxygen-containing functional groups, e. g. phenol-, carboxy- and quinone- type groups, can be electrochemically deprotonated to generate pseudocapacitance.

EIS of B-doped ACs is shown in Fig. 5c. It is obvious that B-doped ACs (BAC-800 and BAC-850) have the lower ESR and steeper curve in the low frequency range, indicating the higher electrical conductivity compared to non-doped sample (AC). In addition, the cycle stability of BAC-850 was tested. After 20,000 cycles, the specific capacitance of BAC-850 still remains 95% of its initial value, as shown in Fig. 5d.

Due to the synergistic effect of the B-N co-doping, B-N co-doped AC (BNAC-850) exhibits an improved electrochemical performance compared to single heteroatom doped ACs. As specifically shown in Fig. 6a and 6b, BNAC-850 shows the highest capacitance of 176 $F \cdot g^{-1}$ at 0.5 $A \cdot g^{-1}$, contributed by electrical double layer capacitance and pseudo- capacitance. Fig. 6c shows that BNAC-850 has a lower resistance than AC. The cycling stability of BNAC-850 was tested in 20,000 cycles at a current density of 1 $A \cdot g^{-1}$ (Fig. 6d). The specific capacitance reaches 118.2% of the initial value after first 2,500 cycles, which may be attributed to the activation process of the electrode material. The electrode of BNAC-850 shows a high capacitance retention rate of 96%. The EIS of all activated carbons were fitted by an electric equivalent circuit model as shown in Fig. 6d (insert). Table 4 shows the fitting values of $R_s$ and $R_{CT}$. BAC-850 exhibits the lowest $R_{CT}$, which indicates that boron doping can enhance the charge transfer rate. BNAC-850 exhibits lower $R_s$ than that of non-doped AC, demonstrating that synergistic effect of B-N co-doping can effectively improve the electrical conductivity of electrode materials.

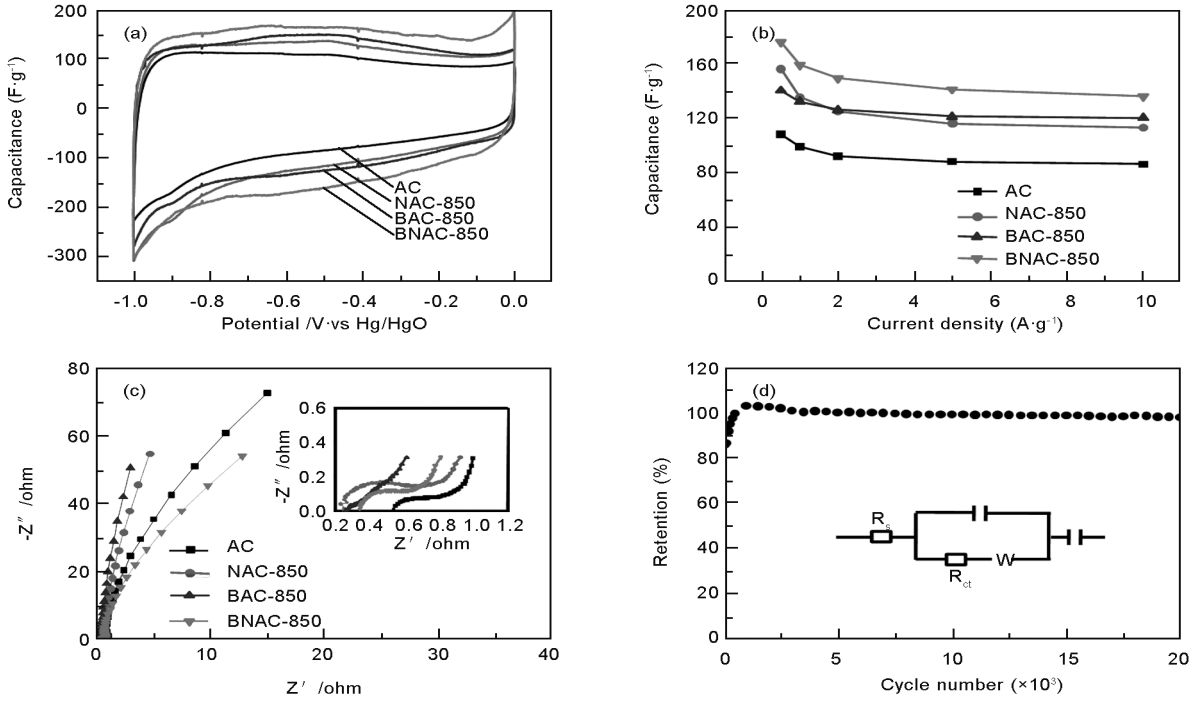


Fig. 6 The electrochemical performances of samples AC, NAC-850, BAC-850 and BNAC-850, (a) CV curves recorded at 5 $mV \cdot s^{-1}$, (b) the specific capacitance as a function of discharging current density, (c) EIS and (d) cycling stability of BNAC-850 at 1 $A \cdot g^{-1}$ (insert: an electric equivalent circuit model).

**Table 4 Resistance of coal-based ACs.**

| Samples | $R_s$/ ohm $cm^{-2}$ | $R_{ct}$/ ohm $cm^{-2}$ |
|---|---|---|
| AC | 0.598 | 0.212 |
| NAC-850 | 0.266 | 0.411 |
| BAC-850 | 0.304 | 0.131 |
| BNAC-850 | 0.361 | 0.256 |

The energy density and power density of BNAC-850 were calculated as 9.7 $Wh \cdot kg^{-1}$ and 2 000 $W \cdot kg^{-1}$, respectively, which are superior to those of recently reported heteroatom doped carbon materials, such as nitrogen-doped porous carbon fibers (7.1 $Wh \cdot kg^{-1}$)[32] and boron and nitrogen co-doped porous carbon (3.8 $Wh \cdot kg^{-1}$)[22]. This superiority can be ascribed to an excellent rate performance of BNAC-850, revealing that this carbon can be

used as an excellent electrode material.

## 4 Conclusions

This study reports a convenient way for the preparation of heteroatom doped ACs using Xinjiang coal as the carbon precursor, melamine as the nitrogen source and boric acid as the boron source. The results reveal that N-doped (NAC-850, NAC-800), B-doped (BAC-850, BAC-800) and B, N-doped (BNAC-850) ACs all give superior electrochemical properties to non-doped one (AC). It is especially worth noting that B, N-doped AC (BNAC-850) gives a capacitance of 176 $F \cdot g^{-1}$ at 0.5 $A \cdot g^{-1}$, which is 63, 12.5 and 25.4% higher than that of AC, NAC-850 and BAC-850, respectively. Also, it has a high energy density of 9.7 $Wh \cdot kg^{-1}$ and power density of 2000 $W \cdot kg^{-1}$. During 20,000 long-term cycles, the electrode of BNAC-850 shows stable capacitance retention and retains 96% of its initial capacitance. Hence, this B-N co-doped AC is an extremely promising material for supercapacitor electrode. Based on the method in this paper, non-caking Xinjiang coal with high carbon and low ash contents is suitable for producing high value added electrode materials in a large scale.

**References**


[1] Wang W, Hao Q L, Lei W, et al. Ternary nitrogen-doped graphene/nickel ferrite/polyaniline nanocomposites for high-performance supercapacitors[J]. J Power Sources 2014, 269: 250-259.

[2] Gao Z, Yang W L, Wang J, et al. A new partially reduced graphene oxide nanosheet/polyaniline nanowafer hybrid as supercapacitor electrode material[J]. Energy Fuels, 2013, 27: 568-575.

[3] Nagamuthu S, Vijayakumar S, Muralidharan G. Synthesis of $Mn_3O_4$/amorphous carbon nanoparticles as electrode material for high performance supercapacitor applications[J]. Energy Fuels, 2013, 27: 3508-3515.

[4] Zhang L L, Zhao X S. Carbon properties and their role in supercapacitors[J]. Chem Soc Rev, 2009, 38: 2520-2531.

[5] Zhai, Y P, Dou Y Q, Zhao D Y, et al. Carbon materials for chemical capacitive energy storage[J]. Adv Mater, 2011, 23: 4828-4850.

[6] Sevilla M, Mokaya R. Energy storage applications of active carbon: supercapacitors and hydrogen storage[J]. Energy Environ Sci, 2014, 7: 1250-1280.

[7] Wang J C, Kaskel S. KOH activation of carbon-based materials for energy storage[J]. J Mater Chem, 2012, 22: 23710-23725.

[8] Yang Y, Zhao B, Tang P, et al. Flexible counter electrodes based on nitrogen-doped carbon aerogels with unable pore structure for high-performance dye-sensitized solar cells[J]. Carbon, 2014, 77: 113-121.

[9] Dong B T, Zhang X, Xu X, et al. Preparation of scale-like nickel cobaltite nanosheets assembled on nitrogen-doped reduced grapheme oxide for high-performance supercapacitors[J]. Carbon, 2014, 80: 222-228.

[10] Hao Q L, Xia X F, Lei W, et al. Facile synthesis of sandwich-like polyaniline/boron-doped grapheme nano hybrid for supercapacitors[J]. Carbon, 2015, 81: 552-563.

[11] Jin H, Wang X M; Gu Z R, et al. A facile method for preparing nitrogen-doped graphene and its application in supercapacitors[J]. J Power Sources, 2015, 273: 1156-1162.

[12] Wang X, Xiao Y, Wang J Q, et al. Facile fabrication of molybdenum dioxide/nitrogen-doped grapheme hybrid as high performance anode material for lithium ion batteries[J]. J Power Sources, 2015, 274: 142-148.

[13] Zhang J F, Nakai T, Uno M, et al. Effect of the boron content on the steam activation of boron-doped diamond electrodes[J]. Carbon, 2013, 65: 206-213.

[14] Li L J, Glerup M, Khlobystov A N, et al. The effects of nitrogen and boron doping on the optical emission and diameters of single-walled carbon nanotubes [J]. Carbon, 2006, 44: 2752-2757.

[15] Wang H Q, Guo Q G, Yang J H, et al. Microstructural evolution and oxidation resistance of polyacrylonitrile-based carbon fibers doped with boron by the decomposition of $B_4C$[J]. Carbon, 2013, 56: 296-308.

[16] Kondo T, Kodama Y, Ikezoe S, et al. Porous boron-doped diamond electrodes fabricated via two-step thermal treatment[J]. Carbon, 2014, 77: 783-789.

[17] Konnoa H, Nakahashia T, Inagakia M, et al. Nitrogen incorporation into boron-doped graphite and formation of B-N bonding[J]. Carbon, 1999, 37: 471-475.

[18] Wu Y P, Fang S B, Jiang Y Y. Carbon anode materials based on melamine resin[J]. J Mater Chem, 1998, 8: 2223-2227.

[19] Wu Y P, Fang S B, Jiang Y Y, et al. Effects of doped sulfur on electrochemical performance of carbon anode[J]. J Power Sources, 2002, 108: 245-249.

[20] Koo′s A, Dillon F, Obraztsova E, et al. Comparison of structural changes in nitrogen and boron-doped multi-walled carbon nanotubes[J]. Carbon, 2010, 48: 3033-3041.

[21] Arutyunyan N R, Arenal R, Obraztsova E D, et al. Incorporation of boron and nitrogen in carbon nanomaterials and its influence on their structure and opto-electronical properties[J]. Carbon, 2012, 50: 791-799.

[22] Guo H L, Gao Q M. Boron and nitrogen co-doped porous carbon and its enhanced properties as supercapacitor[J]. J Power Sources, 2009, 186: 551-556.

[23] Konno H, Ito T, Ushiro M, et al. High capacitance B/C/N composites for capacitor electrodes synthesized by a simple method[J]. J Power Sources, 2010, 195: 1739-1746.

[24] Ma X L, Ning G Q, Sun Y Z, et al. High capacity Li storage in sulfur and nitrogen dual-doped graphene networks[J]. Carbon, 2014, 79: 310-320.

[25] Wang C L, Zhou Y, Sun L, et al. Sustainable synthesis of phosphorus- and nitrogen-co-doped porous carbons with tunable surface properties for supercapacitors[J]. J Power Sources, 2013, 239: 81-88.

[26] Nasini U, Bairi V G, Ramasahayam S K, et al. Phosphorous and nitrogen dual heteroatom doped mesoporous carbon synthesized via microwave method for supercapacitor application[J].

J Power Sources, 2014, 250: 257-265.
[27] Guo D C, Mi J, Hao G P, et al. Ionic liquid $C_{16}$mim$BF_4$ assisted synthesis of poly(benzoxazine-co-resol)-based hierarchically porous carbons with superior performance in supercapacitors [J]. Energy Environ Sci, 2013, 6: 652-659.
[28] Zhong S K, Zhou L H, Wu L, et al. Nitrogen- and boron-co-doped core shell carbon nanoparticles as efficient metal-free catalysts for oxygen reduction reactions in microbial fuel cells[J]. J Power Sources, 2014, 272: 344-350.
[29] Fan X Q, Zhang L X, Zhang G B, et al. Chitosan derived nitrogen-doped microporous carbons for high performance $CO_2$ capture[J]. Carbon, 2013, 61: 423-430.
[30] Yang L J, Jiang S J, Zhao Y, et al. Boron-doped carbon nNanotubes as metal-free electrocatalysts for the oxygen reduction reaction[J]. Angew Chem Int Ed Eng, 2011, 123: 7270-7273.
[31] Panchakarla L S, Govindaraj A C, Rao N R. Nitrogen-and boron-doped double-walled carbon nanotubes [J]. ACS Nano, 2007, 1: 494-500.
[32] Chen L F, Zhang X D, Liang H W, et al. Synthesis of nitrogen-doped porous carbon nanofibers as an efficient electrode material for supercapacitors[J]. ACS Nano, 2012, 8: 7092-7102.
[33] Ghosh A, Lee Y H. Carbon-based electrochemical capacitors [J]. ChemSusChem, 2012, 5: 480-499.
[34] Chen H, Zhou S X, Chen M, et al. Reduced graphene Oxide-$MnO_2$ hollow sphere hybrid nanostructures as high-performance electrochemical capacitors[J]. J Mater Chem, 2012, 22: 25207-26216.
[35] Wang D W, Li F, Chen Z G, et al. Synthesis and electrochemical property of boron-doped mesoporous carbon in supercapacitor [J]. Chem Mater, 2008, 20: 7195-7200.
[36] Han J W, Zhang L L, Lee S, et al. Generation of B-doped graphene nanoplatelets using a solution process and their supercapacitor applications[J]. ACS Nano, 2013, 7: 19-26.
[37] Iyyamperumal E, Wang S Y, Dai L M. Vertically aligned BCN nanotubes with high capacitance[J]. ACS Nano, 2012, 6: 5259-5265.

# 《新型炭材料》2015 年 ~ 2016 年优秀论文评选结果揭晓

经《新型炭材料》编辑、顾问委员会全体成员无记名投票,按得票多少选出《新型炭材料》2015 年 ~ 2016 年优秀论文如下:

2015 年

| No | 姓 名 | 所在单位 | 文 章 标 题 | 期:页码 |
|---|---|---|---|---|
| 1 | 王 琴等 | 北京建筑大学 | 氧化石墨烯对水泥基复合材料微观结构和力学性能的影响 | 4: 349-356 |
| 2 | 吴明铂等 | 中国石油大学 | 微波法制备电化学电容器用花生壳基活性炭 | 1: 86-91 |
| 3 | 杨真真等 | 上海理工大学 | $CaCl_2$ 催化 $NaBH_4$ 还原氧化石墨烯 | 1: 41-47 |
| 4 | 吴雪平等 | 合肥工业大学 | 凹凸棒石/炭对低浓度亚甲基蓝的吸附性能 | 1: 71-78 |
| 5 | 李 晨等 | 中国科学院电工研究所 | 三维石墨烯网络在超级电容器中的应用 | 3: 193-206 |
| 6 | 张向倩等 | 大连理工大学 | 多孔炭材料的设计合成及 $CO_2$ 吸附分离研究进展 | 6: 481-501 |
| 7 | 任桂知等 | 纤维材料改性国家重点实验室 | 拉曼光谱分析炭纤维表面的微观结构 | 5: 476-480 |
| 8 | 刘国强等 | 清华大学 | GO/MOF 复合材料的制备及其吸附苯和乙醇性能 | 6: 566-571 |

2016 年

| No | 姓 名 | 所在单位 | 文 章 标 题 | 期:页码 |
|---|---|---|---|---|
| 1 | 谢莉婧等 | 中国科学院山西煤炭化学研究所 | 基于 CoNi-双金属氢氧化物//AC 非对称超级电容器的构筑 | 1: 37-45 |
| 2 | 郭梦清等 | 清华大学 | 多孔掺磷碳纳米管:磷酸水热合成及其在氧还原和锂硫电池中的应用 | 3: 352-362 |
| 3 | 刘立乐等 | 福州大学 | 多孔 $CuCo_2S_4$/石墨烯复合材料的合成及其在超级电容器上的应用 | 3: 336-342 |
| 4 | 马 朗等 | 同济大学 | 原位聚合法与溶液混合法制备石墨烯/聚酰亚胺复合材料及其性能 | 2: 129-134 |
| 5 | 郑冰娜等 | 浙江大学 | 聚苯胺复合石墨烯纳米卷的制备及其在超级电容器中的应用 | 3: 315-320 |
| 6 | 邵姣婧等 | 贵州大学 | 二维纳米材料的自上而下制备:可控液相剥离 | 2: 97-114 |
| 7 | 刘洪阳等 | 中国科学院金属研究所 | 快速积炭法制备形貌可控的中空纳米炭材料 | 1: 87-91 |
| 8 | 谭明慧等 | 中国石油大学 | 超级电容器用高性能石油焦基多孔炭的制备及改性 | 3: 343-351 |

《新型炭材料》编辑部

2017 年 10 月